CrossMark

ORIGINAL ARTICLE

Brazilian disk test and digital image correlation: a methodology for the mechanical characterization of brittle materials

E. Sgambitterra · C. Lamuta · S. Candamano · L. Pagnotta

Abstract In this paper, an optimized and reliable approach for the evaluation of the mechanical properties of brittle materials is proposed and applied to the characterization of geopolymer mortars. In particular, the Young's modulus, the Poisson's ratio and the tensile strength are obtained by means of a Brazilian disk test combined with the digital image correlation (DIC) technique. The mechanical elastic properties are evaluated by a special routine, based on an over-deterministic method and the least square regression, that allows to fit the displacement fields experienced by the samples during the experiment. Error sources, like center of the disk location and rigid-body motion components, were analyzed and estimated automatically with the proposed procedure in order to perform an accurate evaluation of the elastic constants. The strain field measured by DIC and the computed elastic properties were then used to perform a local stresses analysis. This latter was exploited to investigate the failure mechanisms and to evaluate the tensile strength of the investigated material and the obtained data were compared with those predicted by the ASTM and ISMR standards. Three different loading platens (flat, rod and curved) were adopted for the Brazilian test in order to evaluate their effect on the elastic properties calculation, on the failure mechanisms and tensile strength evaluation. Results reveal that the curve platens are the most suitable for the tensile strength calculation, whereas the elastic properties did not show any influence from the loading configuration. Furthermore, the proposed procedure, of easy implementation, allows to accurately calculate Young's modulus, Poisson's ratio and the tensile strength of brittle materials in a single experiment.

Keywords Brazilian disk test · Digital image correlation · Young's modulus · Poisson's ratio · Tensile strength · Inverse problem · Geopolymer

E. Sgambitterra · C. Lamuta · L. Pagnotta
Department of Mechanical, Energy and Management Engineering - DIMEG, University of Calabria, Ponte P. Bucci, cubo 44C, 87030 Arcavacata di Rende, CS, Italy

C. Lamuta
Beckman Institute for Advanced Science and Technology, University of Illinois at Urbana-Champaign, Urbana, IL 61801, USA

S. Candamano (✉)
Department of Environmental and Chemical Engineering - DIATIC, University of Calabria, Ponte P. Bucci, cubo 44A, 87030 Arcavacata di Rende, CS, Italy
e-mail: sebastiano.candamano@unical.it

rilem

1 Introduction

The Brazilian test [1, 2] is a technique used to evaluate the tensile strength of brittle materials like concrete or rocks. The experiment consists in compressing a circular disk along its vertical diameter in order to induce tensile failure at the center of the disk. The standardized procedure, together with the suggested dimensions of the samples, that allows to calculate the tensile strength of brittle materials, is proposed by the ASTM C496 Standard [3]. However, it is important to underline that the identification of the correct size of the sample, as well as the shape of the loading platens and the type of failure during a Brazilian test is still an open issue [4–6]. Recent studies [7, 8] demonstrated that failure mechanisms are highly dependent upon the loading method used. In particular, it was shown that, for small angles of load contacting area, failure occurs far away from the center of the disk, as a consequence of the high local stress induced by the contact loading platens [4].

The ASTM standard recommends flat platens for the application of the mechanical load and a thickness/diameter (t/D) ratio of the sample ranging between 0.2 and 0.75 [3]; however such recommendations were widely criticized because they often induced failure at the loading points rather than at the center of the disk, where the maximum theoretical tensile stress is localized [6, 9]. In contrast, the ISRM recommends curved platens to apply the load, with a radius 1.5 times that of the sample, whose t/D ratio should be 0.5 [10]. In addition, a modified flattened Brazilian disk that ensures failure at the center of the disk was proposed in [9].

Brazilian test was also proposed as a valid alternative for measuring the elastic mechanical properties of brittle materials [11, 12]. In particular, the inverse method [11] and an over-deterministic approach [12] were implemented to fit the experimental displacements, calculated by means of the Moiré interferometry, to the theoretical solution, in order to simultaneously determine two elastic constants (i.e., Young's modulus, E, and Poisson's ratio, v). However, it is worth noting that the application of interferometric optical techniques, for in-plane displacement and deformation measurements, requires special equipment, longtime preparation and stringent stability requirements.

Therefore, most recently, the digital image correlation technique was used in supporting the characterization of brittle materials [13–15]. In particular, the principle and performances of the local digital image correlation (DIC) technique adapted to study local discontinuities in brittle material is reported in [13]. A new method, based on digital image correlation, is introduced in [14] for measuring crack extension in brittle materials. Finally, the application of DIC as a substitute to more traditional strain gauges in Brazilian testing was demonstrated in [15]. All these works highlighted that the DIC offers special and attractive advantages if compared to the most common interferometric optical methods, such as simple experimental setup and specimen preparation, low requirements in measurement, wide range of sensitivity and resolution. Thus, it results more suitable for experiments in conventional testing laboratories.

The implementation of the DIC method is based on simple steps: (1) specimen and experimental preparations; (2) recording images of the specimen surface before and after the application of the load and, finally, (3) processing the acquired images using a computer program to obtain the desired displacement and strain information.

However, only few studies [16, 17] were devoted to evaluate the elastic constants of materials by using the DIC technique during a Brazilian test. In particular, a revisit of the Brazilian disk specimen as a tool for determining elastic constants was proposed in [16]. A fitting procedure was also adopted to calculate the elastic parameters, but it is based on the one dimensional analysis of the displacements measured on the horizontal and vertical diameter of the disk. Furthermore, only one loading configuration was investigated. In [17], an application of the digital image correlation technique, combined with the linear regression approach, is presented to determine the elastic properties of polycarbonate by analyzing the Brazilian disk test. However, it is important to point out that linear analysis can be done only when the effective coordinates of the disk center are known. In fact, displacements provided by correlation software are related to a reference system that is different from the disk center and, therefore, a coordinate change should be done. Usually the physical location of the disk center is identified by the digital images captured during the load history, but if its coordinates are not the effective one estimation errors can occur.

In this context, an optimized and reliable approach to obtain the elastic tensile properties of brittle materials by combining Brazilian test and DIC technique is proposed and applied to the mechanical characterization of geopolymeric specimens.

The digital image correlation technique was used to obtain the full displacement field on the geopolymeric disk surface and a numerical procedure, based on an over-deterministic method and the least square regression, was used to calculate the elastic constants from the measured displacements.

In order to perform an accurate evaluation of the elastic properties, a proper procedure, able to automatically identify the disk center location and rigid body motions, was developed with the aim to delete their error effect on the final solution. To this aim a non-linear regression methodology was implemented and applied.

Once the elastic properties were computed, a local stress analysis was performed, starting from the DIC measured strains, with the aim to calculate the effective stress field experienced by the samples during the load history and the effective tensile strength of the investigated material. Results were compared with the prediction of the analytical solution proposed in literature [3]. Local stresses were also analyzed to investigate the failure mechanisms of the disks. Three different loading platens were adopted in order to evaluate their effect on the elastic properties calculation, on the failure mechanisms and strength of the investigated material. Results were compared with data obtained from 4 points bending tests.

Overall, the paper outlines a methodology to characterize the tensile properties of a brittle material where the driving force is represented by the determination of the full displacement fields experienced by a disk under compression. Such procedure provides a wealth of information including the effective elastic modulus, Poisson's ratio and the automatic localization of the disk center. Furthermore, starting from the strain measurements and the computed elastic properties, the stress distribution experienced by the disk during the load history can be obtained and a direct evaluation of the tensile strength can be done.

The methodology was validated on a geopolymer but it can be applied to any kind of brittle material. Therefore, all the guidelines to perform this kind of characterization are reported and discussed.

2 Methodology

2.1 The least square methods applied to the displacement fields of a Brazilian disk

Figure 1 shows a Brazilian disk under the application of a compression load P. The horizontal (u_x) and vertical (u_y) displacement field experienced by a generic point $Q(x, y)$ when the disk is in plane stress condition, can be expressed as follow [18]:

$$u_x = \frac{1}{E} K_{1x} + \frac{v}{E} K_{2x} \tag{1}$$

$$u_y = \frac{1}{E} K_{1y} + \frac{v}{E} K_{2y} \tag{2}$$

where E is the Young's modulus and v is Poisson's ratio. K_{1x}, K_{2x}, K_{1y} and K_{2y} are parameters dependent upon the load P, the disk dimensions (thickness t and diameter D), and upon the coordinates (x and y). In particular, they can be expressed as follow:

$$K_{1x} = -\frac{P}{\pi t}\left[(\theta_1 + \theta_2) - \frac{1}{2}\sin(2\theta_1) - \frac{1}{2}\sin(2\theta_2) - \frac{2x}{D} \right] \tag{3}$$

$$K_{1y} = -\frac{P}{\pi t}\left[2ln\left(\frac{r_2}{r_1}\right) + \frac{1}{2}\cos(2\theta_1) - \frac{1}{2}\cos(2\theta_2) - \frac{2y}{D} \right] \tag{4}$$

$$K_{2x} = \frac{P}{\pi t}\left[(\theta_1 + \theta_2) + \frac{1}{2}\sin(2\theta_1) + \frac{1}{2}\sin(2\theta_2) - \frac{2x}{D} \right] \tag{5}$$

$$K_{2y} = -\frac{P}{\pi t}\left[\frac{1}{2}\cos(2\theta_1) - \frac{1}{2}\cos(2\theta_2) + \frac{2y}{D} \right] \tag{6}$$

where

$$\theta_1 = \tan^{-1}\left[\frac{(x - x_0)}{\frac{D}{2} - (y - y_0)} \right] \tag{7}$$

$$\theta_2 = \tan^{-1}\left[\frac{(x - x_0)}{\frac{D}{2} + (y - y_0)} \right] \tag{8}$$

$$r_1 = \sqrt{(x - x_0)^2 + \left[\frac{D}{2} - (y - y_0)\right]^2} \tag{9}$$
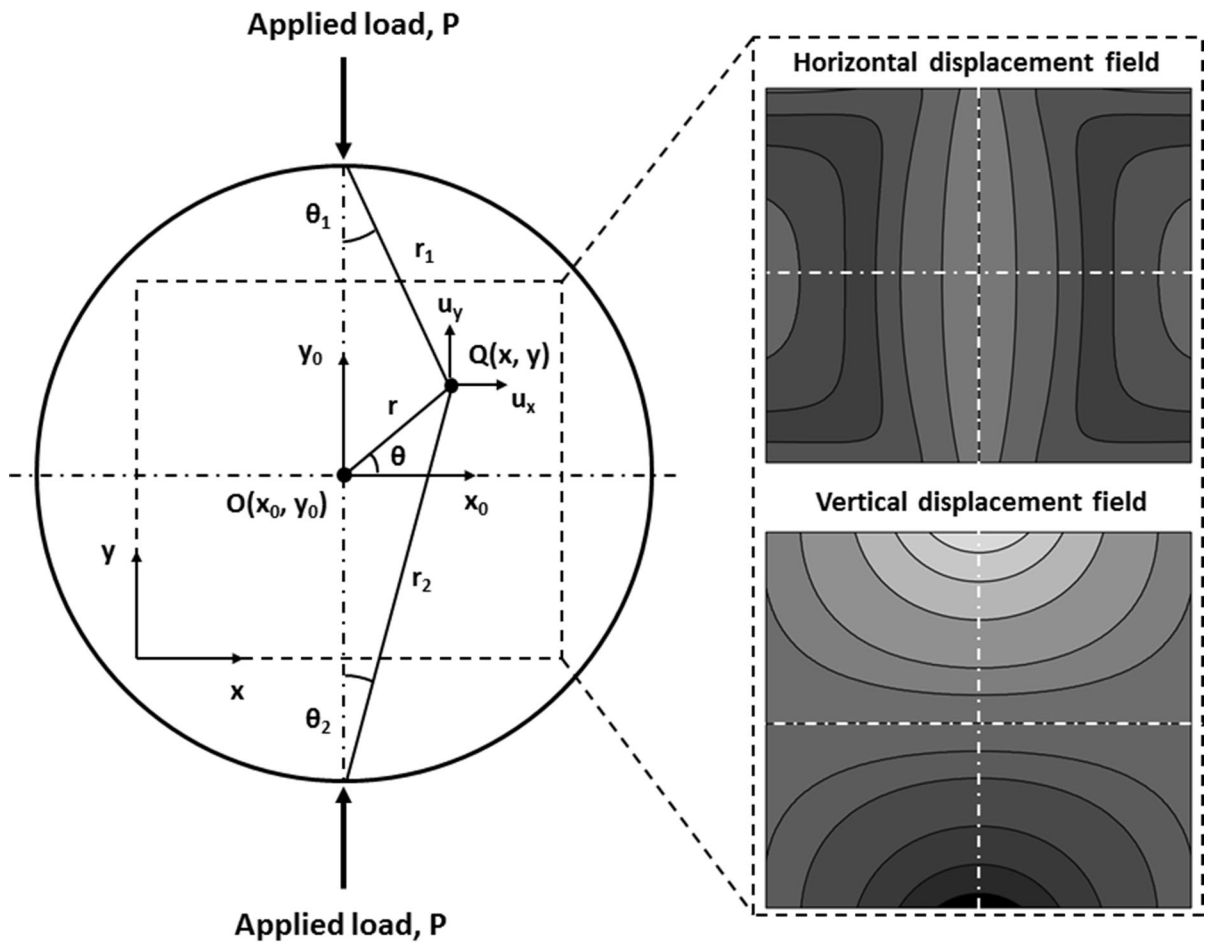
Fig. 1 Schematic depiction of a Brazilian disk subjected to a compression load P

$$r_2 = \sqrt{(x - x_0)^2 + \left[\frac{D}{2} + (y - y_0)\right]^2} \qquad (10)$$

x_0 and y_0 are the coordinates of the disk center.

Equations (1, 2) show that $1/E$ ratio and v are linearly coupled, therefore, if the displacements are known, they can be simultaneously calculated using either the u_x or the u_y displacement field or combining both of them. In particular, if both the u_x and u_y displacement of a generic single point is known, Eqs. (1) and (2) can be easily solved to calculate Young's modulus and the Poisson's ratio parameter. Instead, if the only u_x displacement or the u_y displacement is known you need two points to evaluate both the elastic constants. If the latter is the case, these points must be selected in such a way that the obtained equations are linearly independent, in

order to avoid ill-conditioning that could significantly affect the final result.

To limit such mathematical problem a better way is to use an over-deterministic method which basically makes use of a large number of data points to calculate a small set of unknown coefficients from a large system of equations. Therefore, measuring the whole displacement field of the disk, many equations as much are the investigated points can be written and an overdetermined system of equations can be obtained. In this way, ill-conditioning and unavoidable measurement errors are significantly reduced.

The overdetermined system can be solved using the least square regression (LSR) approach. The least square is a numerical method widely used to find or estimate the values of some unknown parameters (A_i) in order to fit a function to a set of data (F) and to characterize the statistical properties of estimates.

$$F(a_1, a_2, \ldots, a_N) = \sum_{i=1}^{n} A_i f_i(a_1, a_2, \ldots, a_N) \qquad (11)$$

where $(a_1, a_2, \ldots, a_N)$ are the independent variables of the known f_i functions and the unknown A_i coefficients are taken to be independent of the f_i's. If f_j^* is data valuated at $(a_{1j}, a_{2j}, \ldots, a_{Nj})$ then the error between the parameter of interest and the measured data at each jth independent variable can be defined as:

$$\pi_j = \left[\sum_{i=1}^{n} A_i f_i(a_{1j}, a_{2j}, \ldots, a_{Nj}) - f_j^*(a_{1j}, a_{2j}, \ldots, a_{Nj}) \right]^2$$
$$(12)$$

The total error for the entire domain (m) can be written as follow:

$$\pi_{\text{tot}} = \sum_{j=1}^{m} \pi_j = \sum_{j=1}^{m}$$
$$\times \left[\sum_{i=1}^{n} A_i f_i(a_{1j}, a_{2j}, \ldots, a_{Nj}) - f_j^*(a_{1j}, a_{2j}, \ldots, a_{Nj}) \right]^2$$
$$(13)$$

Since the f_i's have been taken to be known functions of the independent variables $(a_{1j}, a_{2j}, \ldots, a_{Nj})$, then the total error is related only to the coefficients, A_i. In order to minimize the error, the partial derivation of the total error with respect to the coefficients are taken and set equal to zero as follows:

$$\frac{\partial \pi_{\text{tot}}}{\partial A_k} = 0 \rightarrow \sum_{j=1}^{m}$$
$$\times \left\{ 2 \left[\sum_{i=1}^{n} A_i f_i(a_{1j}, a_{2j}, \ldots, a_{Nj}) - f_j^*(a_{1j}, a_{2j}, \ldots, a_{Nj}) \right] \right.$$
$$\left. f_i(a_{1j}, a_{2j}, \ldots, a_{Nj}) \right\} = 0 \qquad (14)$$

Solution of the n equations for the unknown A_i forces the "best" possible analytical representation of the measured data, in the sense of minimizing the least square error function.

If data of interest $F(a_1, a_2, \ldots, a_N)$ are represented by the displacements u_x and u_y experienced by a Brazilian disk during the experiment, starting from the well-known stress solutions, see Eqs. (1, 2), they can be efficiently used to calculate the unknown mechanical properties of a material.

In this case it is possible to write that:

$$\begin{bmatrix} u_{xj} \\ u_{yj} \end{bmatrix} = \begin{bmatrix} K_{x1j} & K_{x2j} \\ K_{y1j} & K_{y2j} \end{bmatrix} \begin{bmatrix} \dfrac{1}{E} \\ \dfrac{v}{E} \end{bmatrix} \qquad (15)$$

If u_{xj}^* and u_{yj}^* are the known displacements located at position (x_j, y_j), then the error between the parameter of interest and the measured displacement at each particular point can be defined as:

$$\pi_j = \left[\sum_{i=1}^{2} A_i K_{xi}(x_j, y_j) - u_{xj}^*(x_j, y_j) \right]^2$$
$$+ \left[\sum_{i=1}^{n} A_i K_{yi}(x_j, y_j) - u_{yj}^*(x_j, y_j) \right]^2$$
$$(16)$$

where $A_1 = 1/E$ and $A_2 = v/E$. The total error for the entire domain can be written as follow:

$$\pi_{\text{tot}} = \sum_{j=1}^{m} \pi_j$$
$$= \sum_{j=1}^{m} \left\{ \left[\sum_{i=1}^{n} A_i K_{xi}(x_j, y_j) - u_{xj}^*(x_j, y_j) \right]^2 \right. \qquad (17)$$
$$\left. + \left[\sum_{i=1}^{n} A_i K_{yi}(x_j, y_j) - u_{yj}^*(x_j, y_j) \right]^2 \right\}$$

By minimizing the error, using $\partial \pi_{\text{tot}}/\partial A_i$, it is possible to calculate the elastic constant of the disk.

For the over-deterministic approach, it is desired to use data of all the point of the disk, because more data can reduce random noise and provide more accurate results. However, it is worth noting that the theoretical solution is based on a point load, whereas in typical experiments the load platens generate a distributed pressure on the contact region. In the last years, several studies were carried out in order to provide analytical solutions dependent on the load configuration [19, 20] and it was demonstrated that the displacement field, compared with the solution described in the Eqs. (1, 2), does not significantly change if a region, far away from the contact point, is considered. If the latter is the case, there is no need to use more complex equations [19, 20] to describe the displacement experienced by the disk during the experiment.

In order to verify this aspect, finite element simulations were carried out applying different load distributions [20], and results revealed that the proposed regression method, based on Eqs. (1, 2) is not affected by the load configuration.

Furthermore, it has to point out that the theoretical displacements near the loading area can be different from the experimental data because of the plastic deformations induced by high-localized stresses.

For all of these reasons, the central part of the disk, sufficiently far from the loading regions (dashed rectangle in Fig. 1), was analyzed for least-squares calculation, by assuming that in this region the elastic mechanical properties of the analyzed material are constant, as predicted by the theoretical solution.

2.2 Error sources analysis: elimination of rigid body motions and identification of the disk center location

Equations (1, 2) represent the solution of the displacements of a Brazilian disk calculated with respect to its center. Furthermore, the solution is related to a symmetric load with no rigid translation and/or rotation. When dealing with experiments, such conditions can be lost and, therefore, technical considerations have to be done when the proposed method is implemented. In particular, in order to reduce the effect of unavoidable source of errors, rigid body motions involved during the experiment and the correct disk center location have to be calculated.

The exact position of the center of the disk has to be correctly identified in order to get a good fitting between the experimental and regressed data and to well estimate the elastic constants of the material. In fact, the experimental displacements, provided by a commercial software for the image correlation, are typically related to a reference system that is different from the disk center. Accordingly, it is mandatory identify such a point and make a coordinate change.

Furthermore, during the experiment the disk can be subjected to unavoidable rigid body motions that can significantly affect the elastic constant calculation. Thus, it is of great interest to estimate their values and delete their influence on the final solution.

Rigid body motions can be easily added in Eq. (15) as follows:

$$\begin{bmatrix} u_{xj} \\ u_{yj} \end{bmatrix} = \begin{bmatrix} K_{x1j} & K_{x2j} \\ K_{y1j} & K_{y2j} \end{bmatrix} \begin{bmatrix} \dfrac{1}{E} \\ \dfrac{v}{E} \end{bmatrix} + A \begin{bmatrix} -r_j \sin\theta_j \\ r_j \cos\theta_j \end{bmatrix} + \begin{bmatrix} B_{ux} \\ B_{uy} \end{bmatrix} \tag{18}$$

where B_{ux} and B_{uy} represent the horizontal and vertical rigid translation, respectively, A is the rigid body rotation, $r = \sqrt{(x - x_0)^2 + (y - y_0)^2}$ and $\theta = \tan^{-1}[(y - y_0)/(x - x_0)]$, see Fig. 1.

It is important to underline that the introduction of the latter parameters does not represent an issue for the implementation of the over-deterministic method because the new terms are linearly coupled with respect to the main function and the number of data, provided by the correlation technique, are still higher than the number of constant to calculate.

The estimation of the disk center, instead, cannot be done with a least square regression approach because x_0 and y_0 are not linearly coupled with respect to the main function. To calculate these new parameters, an iterative procedure based on Newton–Raphson method is employed. To this aim Eq. (18) has to be written as a series of iterative equations based on Taylor's series expansions as follows:

$$\begin{aligned} (u_{xj})_{i+1} = (u_{xj})_i &+ \left(\frac{\partial u_{xj}}{\partial \frac{1}{E}}\right)_i \Delta\frac{1}{E} + \left(\frac{\partial u_{xj}}{\partial \frac{v}{E}}\right)_i \Delta\frac{v}{E} \\ &+ \left(\frac{\partial u_{xj}}{\partial A}\right)_i \Delta A + \left(\frac{\partial u_{xj}}{\partial B_{ux}}\right)_i \Delta B_{ux} \\ &+ \left(\frac{\partial u_{xj}}{\partial x_0}\right)_i \Delta x_0 + \left(\frac{\partial u_{xj}}{\partial y_0}\right)_i \Delta y_0 \end{aligned} \tag{19}$$

$$\begin{aligned} (u_{yj})_{i+1} = (u_{yj})_i &+ \left(\frac{\partial u_{yj}}{\partial \frac{1}{E}}\right)_i \Delta\frac{1}{E} + \left(\frac{\partial u_{yj}}{\partial \frac{v}{E}}\right)_i \Delta\frac{v}{E} \\ &+ \left(\frac{\partial u_{yj}}{\partial A}\right)_i \Delta A + \left(\frac{\partial u_{yj}}{\partial B_{uy}}\right)_i \Delta B_{uy} \\ &+ \left(\frac{\partial u_{yj}}{\partial x_0}\right)_i \Delta x_0 + \left(\frac{\partial u_{yj}}{\partial y_0}\right)_i \Delta y_0 \end{aligned} \tag{20}$$

where subscript i denotes the ith iteration step, and $\Delta(1/E)$, $\Delta(v/E)$, ΔA, ΔB_{ux}, ΔB_{uy}, Δx_0 and Δy_0 are corrections to the previous estimation of $(1/E)$, (v/E), A, B_{ux}, B_{uy}, x_0 and y_0. The desired result, i.e. that $(u_{xj})_{i+1}$ and $(u_{yj})_{i+1}$ are equal to the experimentally recorded displacements $(u_{x\,\exp})$ and $(u_{y\,\exp})$, respectively, yields the following simultaneous equations with respect to the corrections:

$$\left(u_{x\,\exp}\right) - \left(u_{xj}\right) = +\left(\frac{\partial u_{xj}}{\partial \frac{1}{E}}\right)\Delta\frac{1}{E} + \left(\frac{\partial u_{xj}}{\partial \frac{v}{E}}\right)\Delta\frac{v}{E}$$
$$+ \left(\frac{\partial u_{xj}}{\partial A}\right)\Delta A + \left(\frac{\partial u_{xj}}{\partial B_{ux}}\right)\Delta B_{ux}$$
$$+ \left(\frac{\partial u_{xj}}{\partial x_0}\right)\Delta x_0 + \left(\frac{\partial u_{xj}}{\partial y_0}\right)\Delta y_0$$

$$(21)$$

$$\left(u_{y\,\exp}\right) - \left(u_{yj}\right) = +\left(\frac{\partial u_{yj}}{\partial \frac{1}{E}}\right)\Delta\frac{1}{E} + \left(\frac{\partial u_{yj}}{\partial \frac{v}{E}}\right)\Delta\frac{v}{E}$$
$$+ \left(\frac{\partial u_{yj}}{\partial A}\right)\Delta A + \left(\frac{\partial u_{yj}}{\partial B_{ux}}\right)\Delta B_{ux}$$
$$+ \left(\frac{\partial u_{yj}}{\partial x_0}\right)\Delta x_0 + \left(\frac{\partial u_{yj}}{\partial y_0}\right)\Delta y_0$$

$$(22)$$

Equations (21, 22) can be written in matrix form:

$$
\begin{bmatrix} u_{x\,\exp} - u_{x1} \\ \vdots \\ u_{x\,\exp} - u_{xm} \\ u_{y\,\exp} - u_{y1} \\ \vdots \\ u_{y\,\exp} - u_{ym} \end{bmatrix}
$$

$$
= \begin{bmatrix}
\frac{\partial u_{x1}}{\partial(1/E)} & \frac{\partial u_{x1}}{\partial(v/E)} & \frac{\partial u_{x1}}{\partial A} & \frac{\partial u_{x1}}{\partial B_{ux}} & 0 & \frac{\partial u_{x1}}{\partial x_0} & \frac{\partial u_{x1}}{\partial y_0} \\
\vdots & \vdots & \vdots & \vdots & \vdots & \vdots & \vdots \\
\frac{\partial u_{xm}}{\partial(1/E)} & \frac{\partial u_{xm}}{\partial(v/E)} & \frac{\partial u_{xm}}{\partial A} & \frac{\partial u_{xm}}{\partial B_{ux}} & 0 & \frac{\partial u_{xm}}{\partial x_0} & \frac{\partial u_{xm}}{\partial y_0} \\
\frac{\partial u_{y1}}{\partial(1/E)} & \frac{\partial u_{y1}}{\partial(v/E)} & \frac{\partial u_{y1}}{\partial A} & 0 & \frac{\partial u_{y1}}{\partial B_{uy}} & \frac{\partial u_{y1}}{\partial x_0} & \frac{\partial u_{y1}}{\partial y_0} \\
\vdots & \vdots & \vdots & \vdots & \vdots & \vdots & \vdots \\
\frac{\partial u_{ym}}{\partial(1/E)} & \frac{\partial u_{ym}}{\partial(v/E)} & \frac{\partial u_{ym}}{\partial A} & 0 & \frac{\partial u_{ym}}{\partial B_{uy}} & \frac{\partial u_{ym}}{\partial x_0} & \frac{\partial u_{ym}}{\partial y_0}
\end{bmatrix}
$$

$$
\begin{bmatrix} \Delta\frac{1}{E} \\ \Delta\frac{v}{E} \\ \Delta A \\ \Delta B_{ux} \\ \Delta B_{uy} \\ \Delta x_0 \\ \Delta y_0 \end{bmatrix}
$$

$$(23)$$

The solution of Eq. (23) in the least-squares sense is

$$[\Delta] = \left([\partial]^{\mathrm{T}}[\partial]\right)^{-1}[\partial]^{\mathrm{T}}[u] \tag{24}$$

The solution of the matrix equation gives the correction terms for prior estimates of the coefficients. Accordingly, an iterative procedure must be used to obtain the best-fit set of coefficients. The procedure described above is repeated until the corrections $[\Delta]$ become acceptably small.

It is important to underline that not expected solutions can be obtained if the initial trial values are far from the effective ones. However, it was observed that if the trial location of the disk center is not far from the real, convergence of the solution is quite quick and results, in terms of elastic constants, are the expected ones.

The latter procedure was numerically validated exploiting the displacement fields obtained from finite element simulations, see Fig. 2b and c. In particular, 2D analysis on a disk with linear elastic properties ($E = 15$ GPa, $v = 0.19$) and diameter $D = 55$ mm were performed. Four-nodes shell elements were used and special care was done in order to guarantee a regular mesh on the central area of the disk, see Fig. 2a, where the proposed method is applied.

Figure 2b and c report the typical horizontal, u_x, and vertical displacement, u_y, respectively. In particular, results are referred to a disk subjected to 1000 N of compression load.

The least squares regression was performed on the measured FEM displacements. Equations (23) were used to fit the numerical data obtained from the simulations and the unknown elastic constant parameters, E and v, were calculated. Results were compared with the elastic properties used in the simulation ($E = 15$ GPa, $v = 0.19$).

Figure 3a and b show that if the correct disk center location is missed, because the used trial value is far from the real one, the numerical displacement contour plots (blue lines) do not match with the analytical one (red line), and the calculated elastic constants will be different from the references ($E = 15$ GPa, $v = 0.19$). Only when the correct disk center location is well identified, displacements show good agreement and the regressed elastic constants are equal to the one used in the FEM model ($E = 15$ GPa, $v = 0.19$).
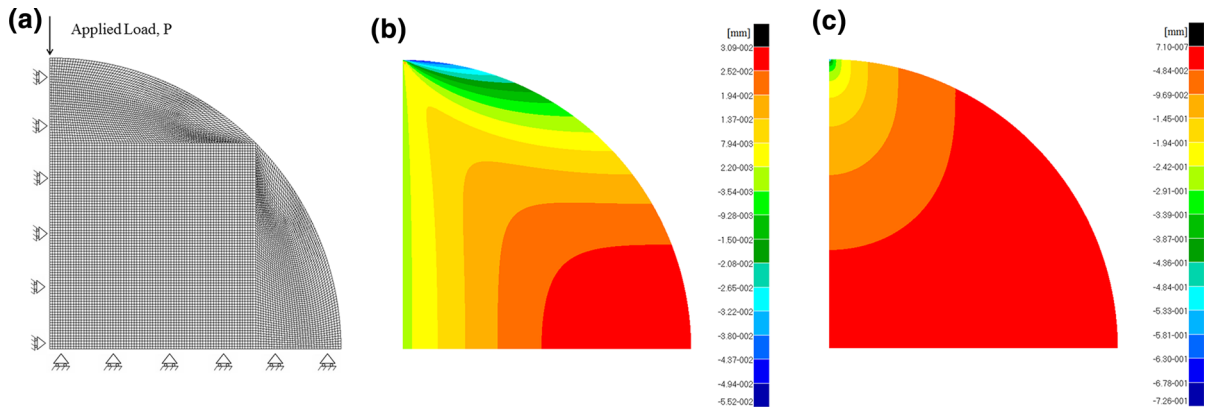
Fig. 2 **a** FEM model; **b** horizontal displacement, u_x; **c** vertical displacement, u_y

3 Stress solution of an isotropic brazilian disk for the tensile strength calculation

The stress solution for an isotropic 2D disk subjected to concentrated loads, Fig. 1, is [21]

$$\sigma_x = \frac{2P}{\pi t}\left(\frac{\cos\theta_1 \sin^2\theta_1}{r_1} + \frac{\cos\theta_2 \sin^2\theta_2}{r_2}\right) - \frac{2P}{\pi Dt} \tag{25}$$

$$\sigma_y = \frac{2P}{\pi t}\left(\frac{\cos^3\theta_1}{r_1} + \frac{\cos^3\theta_2}{r_2}\right) - \frac{2P}{\pi Dt} \tag{26}$$

$$\tau_{xy} = \frac{2P}{\pi t}\left(\frac{\cos^2\theta_1 \sin\theta_1}{r_1} + \frac{\cos^2\theta_2 \sin\theta_2}{r_2}\right) \tag{27}$$

Considering the parameters reported in Fig. 1, the following relationship can be written:

$$r_2^2 = r_2^2 + D^2 - 2r_1 D\cos\theta_1 \tag{28}$$

$$\cos\theta_2 = \frac{D^2 + r_2^2 - r_1^2}{2r_2 D} = \frac{D - r_1\cos\theta_1}{r_2} \tag{29}$$

$$\sin\theta_2\sqrt{1-\cos^2\theta_2} = \frac{r_1\sin\theta_1}{r_2} \tag{30}$$

$$x = r_1\sin\theta_1 \tag{31}$$

$$y = \frac{D}{2} - r_1\cos\theta_1 \tag{32}$$

Manipulating and substituting Eqs. (28–32) in Eqs. (25–27) we get:

$$\sigma_x = \frac{2P}{\pi t}\left[\frac{\left(\frac{D}{2}-y\right)x^2}{\left(\left(\frac{D}{2}-y\right)^2+x^2\right)^2} + \frac{\left(\frac{D}{2}+y\right)x^2}{\left(\left(\frac{D}{2}+y\right)^2+x^2\right)^2} - \frac{1}{D}\right] \tag{33}$$

$$\sigma_y = \frac{2P}{\pi t}\left[\frac{\left(\frac{D}{2}-y\right)^3}{\left(\left(\frac{D}{2}-y\right)^2+x^2\right)^2} + \frac{\left(\frac{D}{2}+y\right)^3}{\left(\left(\frac{D}{2}+y\right)^2+x^2\right)^2} - \frac{1}{D}\right] \tag{34}$$
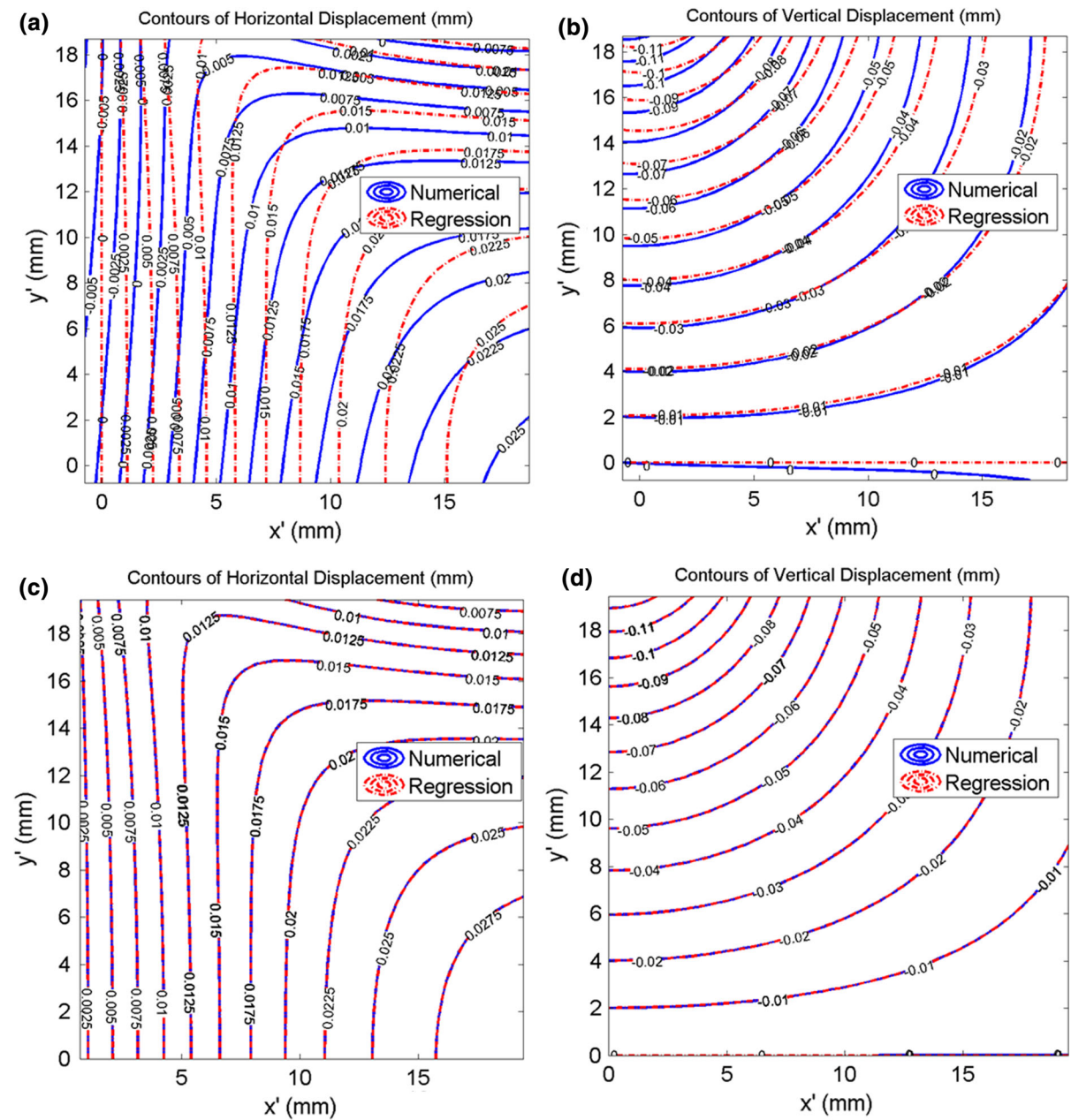
$$\tau_{xy} = \frac{2P}{\pi t}\left[\frac{\left(\frac{D}{2}-y\right)^2 x}{\left(\left(\frac{D}{2}-y\right)^2+x^2\right)^2} + \frac{\left(\frac{D}{2}+y\right)^2 x}{\left(\left(\frac{D}{2}+y\right)^2+x^2\right)^2} - \frac{1}{D}\right] \tag{35}$$

The equations suggested by ASTM and ISMR standards for the calculation of the tensile strength, σ_T, can be obtained from Eq. (33) evaluated at the center of the disk ($x = 0, y = 0$), i.e. where σ_x stress reaches its maximum tensile value.

$$\sigma_T = -\frac{2P}{\pi Dt} \tag{36}$$

It is important to underline that, in geopolymer based mortar disks, the tensile strength leads to the failure because its absolute value is much lower than the one recorded in compression.

Fig. 3 Effect of the disk center location: **a** horizontal displacement u_x for a trial point (x_0, y_0); **b** vertical displacement u_y for a trial point (x_0, y_0); **c** horizontal displacement u_x when the correct center is located; **d** vertical displacement u_y when the correct center is located

4 Experimental setup and procedures

4.1 Material and specimen preparation

Geopolymers were prepared by activating metakaolin with an alkaline silicate solution [22]. Metakaolin, mainly composed by Al_2O_3 (42 %wt) and SiO_2 (53.2 %wt) and with an average particles size of 1.59 μm, a sodium silicate solution of modulus 2.2 and sodium hydroxide (NaOH pellets, 97%, Sigma Aldrich Reagents), were used as reagents.

In order to guarantee good mass transfer and dissolution rate, the maximum extent of metakaolin reaction and aluminium incorporation in geopolymer matrix, the following molar ratios $SiO_2/Na_2O = 1.62$ and $H_2O/Na_2O = 12.25$ were used to prepare the alkaline silicate solution [23, 24]. Firstly, the sodium hydroxide solution was obtained by dissolution of NaOH pellets in ultrapure water, with container kept sealed wherever possible to minimize contamination by atmospheric carbonation and prevent water evaporation. The solution was stirred until the NaOH pellets had dissolved and the solution became clear. During this process, a significant amount of heat is released. So it was allowed to cool back down to room temperature. Once cooled down it was poured into sodium silicate solution. The so obtained alkali activator solution was covered, sealed, stirred. Finally, the activator solution was added to metakaolin powder and the slurry was mechanically vigorously mixed for 10 min. The last step involved sand (< 500 μm) addition and mechanically mixing for 5 min. The slurries were, afterwards, rapidly casted into open Teflon molds with a disk shape (55 mm diameter and thickness/diameter ratio of 0.18), for the Brazilian tests, and a prismatic shape ($135 \times 12 \times 9$ mm^3) for the bending tests and a cube shape ($4 \times 4 \times 4$ cm^3) for the compression tests. A thickness/diameter ratio of 0.18 was chosen for the disk because of technical aspect related to their realization and to keep plane stress conditions for the elastic constants measurements. All samples were vibrated on the vibration table to remove entrained air. In order to prevent the moisture loss, the molds were sealed from the atmosphere and cured for 24 h at 50 °C. The sealed specimens were then stored at ambient temperature and pressure for 4 weeks to complete the curing.

The final theoretical composition of geopolymers has $Al_2O_3\backslash Na_2O$ and $SiO_2\backslash Al_2O_3$ molar ratios in equal to 1 and 3.86 respectively. Molar ratio was fixed equal to one because sodium balances the negative framework charge carried by tetrahedral aluminium, thus acting as structure forming agent. SiO_2/Al_2O_3 molar ratio was fixed to 3.8 in order to minimize geopolymer porosity thus increasing mechanical performance The Water/Binder (W/B) weight ratio was fixed at 0.56 to obtain a good mortar workability. Sand/Binder (S/B) $= 1.5$ has been used to avoid the risk of microcracks due to shrinkage.

The produced material was characterized by means of different analysis (i.e., XRD, NMR, SEM), and results are shown in the Supplementary Materials documentation.

4.2 Brazilian disk experiments and DIC measurements

Brazilian test experiments were performed using an electro-mechanical testing machine (MTS Criterion c42, USA) equipped with a 5 kN load cell. All the experiments were carried out in displacement control with a speed of 0.05 mm/min using three different loading platens. In particular, flat platens, rod platens with 10 mm of diameter and curved platens with 42.5 mm of radius (see Figure S2) were employed. Figure S2 also reports a typical mechanical load–displacement response of a tested disk. All the correlation measurements were performed in the linear region of the load–displacement response. In particular, the first image in the measurement test (point 1 in Figure S2) was used as the reference one, and terms up to first order displacement gradients were used in all the analyses. Digital image correlation was used to obtain full-field displacements of each image throughout the test (n-points in Figure S2). The whole experimental setup, including the testing machine, was placed on an anti-seismic platform to avoid measurements errors due to unavoidable vibrations.

Six samples for each load condition were investigated and all of them were painted with white and black paint in order to get a proper pattern with a random grey scale distribution.

A digital camera (Sony ICX 625- Prosilica GT 2450 model) with a resolution of 2448 by 2050 pixels was used to capture images throughout measurement tests. The focus of the images was performed using a Linos Photonics objective and a Rodagon lens f. 80 mm. Furthermore, camera spacers were adopted in order to get the magnification allowing the visualization of the entire disk. In these conditions a scale of approximately 35 pixels/mm was obtained.

Digital image correlation was performed on images captured from each test by setting 71 pixels for the subset size and 5 pixels for the step size. A commercially available image correlation software (Vic-2D Correlated Solution) was employed for the analyses. This latter, in typical setups as the one used for this work, has an in-plane displacement accuracy of 1/

50,000 of the field of view. However, because of the variability in noise level from test-to-test, it is often beneficial to examine the noise level on the measured displacement field for the specific test. To this aim, a set of five or more images was taken, over the same region of interest, on a sample under zero load condition, without varying the speckle pattern parameter, as suggested in [25]. Under such conditions, the real displacement from one image to the next should be zero. However, due to the experimental noise, a small displacement, different from zero, is detected by the software, with an average value of 1.4 μm in the entire region of interest. The standard deviation between the small displacements measured for every image was calculated and a value of 0.15 μm was obtained. Such value represents the uncertainty of the displacement measurements carried out by the DIC and its influence on the estimation of the elastic constants has been studied. In particular, the standard deviation of the Young's modulus and Poisson's ratio, starting from the uncertainty of the displacements, has been measured as follows: (1) the displacement field measured during an experiment was selected; (2) a field of random numbers, lying in the range defined by the uncertainty of the displacements (i.e., 1.4 ± 0.15 μm), was generated according to a Gaussian distribution and it was added, as an error, to the displacement field previously selected; (3) the new "wrong" displacements were used to evaluate the new "wrong" elastic constants by means of Eq. (23); (4) after repeating steps (2) and (3) several times, the standard deviation of the previously obtained values of E and v was calculated. This latter represents the uncertainty of the elastic constants generated by the experimental noise affecting the displacements measured by the DIC. In our experiments, a standard deviation of 18.25 MPa and $5.87 \cdot 10^{-4}$ was obtained for E and v, respectively, demonstrating that, with the adopted setup, elastic constants variables are not significantly affected by the displacement noise.

4.3 Bending test

Four points bending tests (4-PBT) were performed according to the ASTM C 1161-02c [26] standard and using an electro-mechanical testing machine (MTS Criterion c42, USA), equipped with a 5kN load cell.

Six prismatic shaped samples with dimensions of $135 \times 12 \times 9$ mm^3 were used to perform these tests. The adopted sizes were selected according to recommendations of the ASTM C 1161-02c standard [26], that, for the proposed configuration C, suggests 90 mm length, 8 mm width and 6 mm thickness. However, since the total width of the used XY strain gauges was higher than 8 mm, a specimen with 12 mm of width was made in order to guarantee a suitable installation of the strain gauges. The values of the length and the thickness were then chosen in order to keep the same length/width, width/thickness and length/thickness ratios suggested by the ASTM C 1161-02c standard.

HBM K-XY3 strain gauges were glued at the center of the lower surface of the samples (i.e. where the maximum tensile stress is localized) and the HBM QuantumX MX1615B Strain Gauge Bridge Amplifier, together with the Catman software, was employed to record longitudinal and transverse strains during the test.

The bending tests were performed with a crosshead speed equal to 1 mm/min, as suggested by the ASTM C 1161-02c standard, and the Poisson ratio v was calculated by editing the strains measured by the XY strain gauge according to the transverse sensitivity of the strain gauges and the Poisson ratio of the material adopted for their calibration [27].

5 Results and discussion

5.1 Elastic constants calculation

The reliability of the proposed approach was validated by the experiments performed on the geopolymeric materials. In particular, the experimental displacements, recorded by means of the correlation software, were used as input parameters of the Eq. (23). Figure 4a and b report representative contours plot of the horizontal, u_x, and vertical, u_y, displacements, respectively, obtained from a sample tested by curved platens. In particular, blue lines represent the experimental displacements after the rigid body motions, A, B_{ux} and B_{uy}, were deleted, whereas red lines are the analytical displacements calculated by using the regressed elastic constants, E and v.

(a)

Contours of Horizontal Displacement (mm)

(b)

Contours of Vertical Displacement (mm)

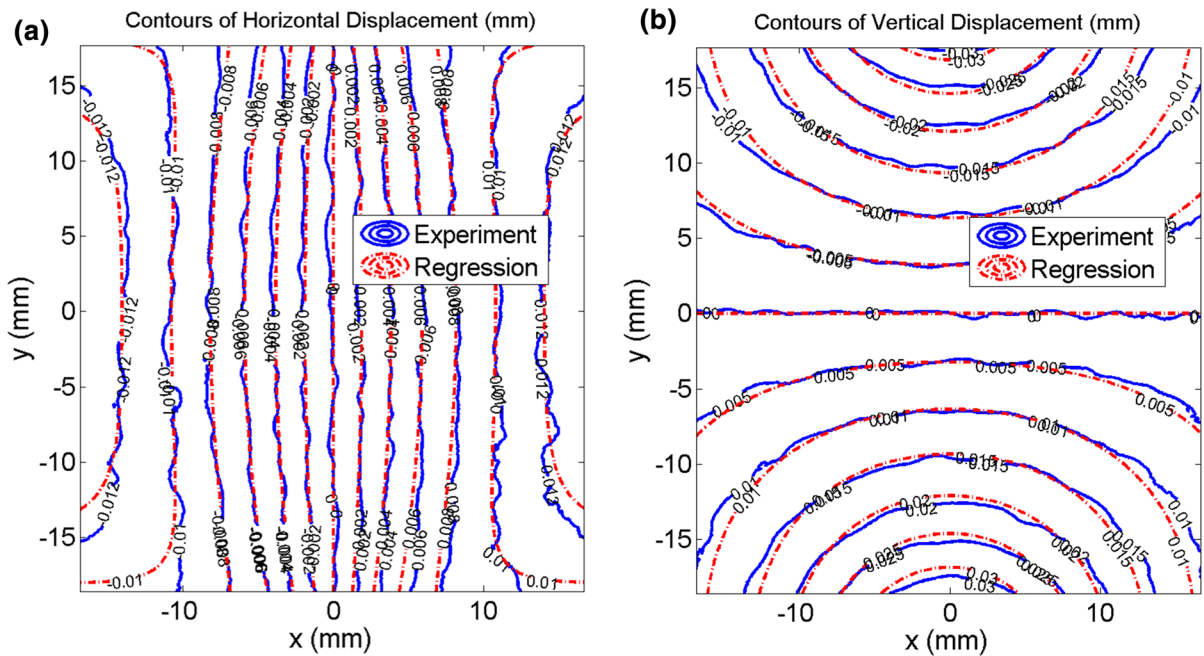**Fig. 4** Comparison between the experimental and regressed displacement fields: **a** horizontal displacements u_x and **b** vertical displacement u_y

Table 1 Tensile elastic constants obtained from four-point bending (4-PBT) tests and least square regression (LSR)

	4-PBT		LSR flat platens (ASTM)		LSR rod platens		LSR curved platens (ISRM)	
	Ave.	St. dev.	Ave.	St. dev.	Ave.	St. dev.	Ave.	St. dev.
Young's modulus, E (GPa)	14.73	0.16	14.33	1.17	14.96	0.83	15.21	1.47
Poisson's ratio, v	0.186	0.004	0.190	0.016	0.197	0.014	0.192	0.025

Results show a very good agreement between the experimental and analytical data. Same behavior was also observed when flat and rod plates were used. As previously discussed, such agreement can be obtained only if the investigation region is far from the loading area (as shown in Fig. 1). In fact, the high stress concentration occurring at the contact point generates big perturbation on the displacement distribution that significantly affects the regression analysis and, consequently, the constants calculation. It is also important to point out that the experimental displacement fields well match the theoretical solution for isotropic material, therefore, assuming constant elastic properties in the entire investigated area, as done in this investigation, can be considered a correct hypothesis.

Regressed elastic constants, for the three loading conditions, together with the ones obtained from the four points bending tests, are reported in Table 1.

Results revealed that the proposed approach is well suitable in evaluating the elastic constants of brittle isotropic material. In fact, a good agreement between results obtained with the regression and the conventional four points bending tests was observed.

One can observe that the values of the standard deviation of the elastic constants related to the different tested samples are higher than the one related to the experimental noise of the DIC measurements, as reported in Sect. 4.2. Considering the highly scattered experimental data, typically obtained from the mechanical characterization of ceramic materials, such as geopolymers, the errors generated by the experimental noise affecting the DIC technique can, in fact, be considered negligible.

In addition, it can be observed that the different loading configurations do not significantly affect the elastic constants estimation. Such behavior can be

Table 2 Tensile strength values measured with the three different loading conditions adopted

	Flat platens (ASTM)		Rod platens		Curved platens (ISRM)	
	Ave.	St. dev.	Ave.	St. dev.	Ave.	St. dev.
Tensile strength, σ_T (MPa)	4.28	0.44	3.17	0.43	5.47	0.68

related to the position of the investigation area that is far from the loading point, where the displacements are significantly affected by high stress concentration.

5.2 Failure analysis and tensile strength evaluation

Stress analysis, to evaluate the effect of the loading platens configuration (flat, rod and curved) on the material strength, was performed. In particular, starting from the mechanical response of the disk, the maximum load, P_{max}, immediately before the failure, was recorded and the tensile strength, σ_T, was calculated by the Eq. (36) according to which failure should occur at the center of the disk.

Results, reported in Table 2, revealed that the highest σ_T is obtained when curved platens are used, whereas the lowest value is recorded when the load is applied using rod platens. This effect is mainly related to the size of the contact area, between the sample and the platens, generated during the application of the load. In fact, curved platens, suggested by the ISRM, guarantee the highest contact area and the lowest stress concentration at the loading points. This conditions allows, with high probability, to get failure at the center of the disk. On the contrary, when rod platens are used, the contact area results very small whereas stress concentration will be extremely high, generating premature failure of the sample. If the latter is the case, no correct estimation of the tensile strength of the material can be obtained because failure does not occur according to the standard.

A local stress analysis was also performed, starting from the measured DIC strain data, in order to get a better interpretation of the obtained results. To this aim, in plane Lagrangian strains, ε_x and ε_y, were calculated from the displacement measurements [25]. The horizontal (σ_x) and the vertical (σ_y) tensile stress distribution were then measured immediately before the failure of the sample for all the loading configurations, according to the plane stress solution:

$$\sigma_x = \frac{E}{1-v^2}\left[\varepsilon_x + v\varepsilon_y\right] \tag{37}$$

$$\sigma_y = \frac{E}{1-v^2}\left[\varepsilon_y + v\varepsilon_x\right] \tag{37}$$

where E and v are the Young's modulus and the Poisson's ratio previously calculated by the regression analysis. For the purposes of comparison, representative tests of each loading method were selected and the obtained results, in terms of σ_x, responsible of the mechanical tensile failure, are reported in Fig. 5. However, further data, obtained from the repetitions of the same experiment, are also reported in Figures S3 and Figure S4, and similar results were obtained. In particular, Fig. 5a, b and c report the contour maps of the horizontal stress field σ_x before failure, together with its evolution along the y axis for the three loading configurations, i.e. flat, rod and curved platens, respectively. Furthermore, figures report a direct comparison of the stress profile (σ_x) with respect to the tensile strength (σ_T) predicted by the Eq. (36), see data reported in Table 1. Results show that when flat platens are used, Fig. 5a, horizontal tensile stress tends to concentrate at the loading points, in fact very high tensile stress level are recorded in these regions. However, it has to point out that also at the center of the disk the recorded tensile stress is close to the analytically predicted but it did not generate failure. Concerning the rod platens, Fig. 5b, results show that the high tensile stresses, responsible of the failure, are only localized at the contact point, whereas low tensile stress, compared with the analytical prediction, is recorded at the center of the disk. Finally, it was observed that, only when loading platens are used, Fig. 5c, the σ_x stress profile is very close to the analytical prediction. In fact, tensile stresses are only recorded at the center of the disk, whereas compression horizontal stresses are observed at the contact points.

In addition, Figures S5 report a direct comparison of the contour maps of the horizontal σ_x and vertical σ_y
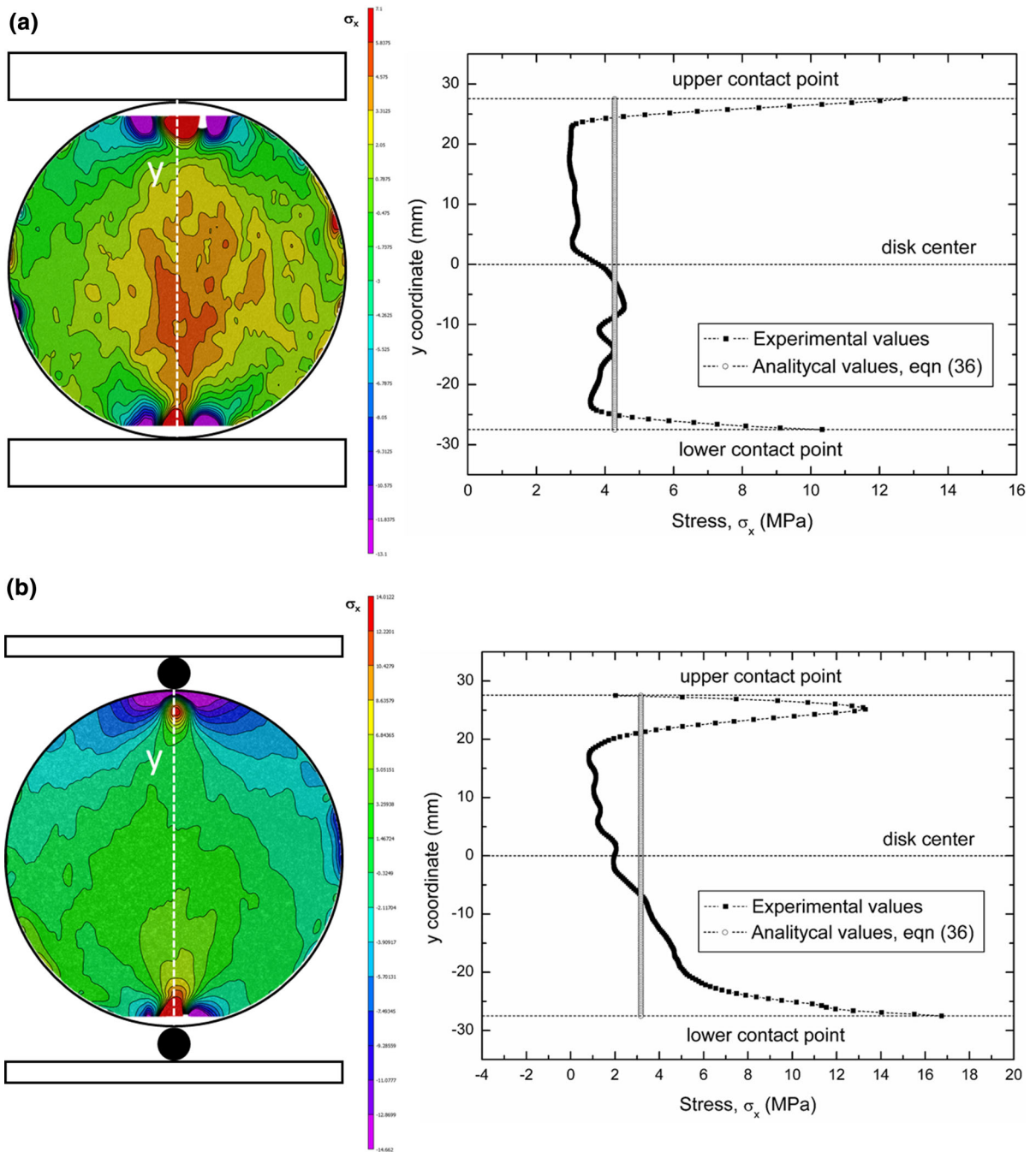
Fig. 5 Local tensile stress (σ_x) distribution immediately prior to the failure for samples loaded with: **a** flat platens; **b** rod platens; **c** curved platens

stress field before failure, for the three different loading conditions.

Qualitative assessment of Figure S5a, shows that the ASTM loading method, highlights two regions of dominant horizontal compression located to the top

and bottom of the disc and a region of dominant tensile stress, responsible of the failure, immediately close to the contact point. Compressive vertical stress, caused by loading the top and bottom points of the disc, can be clearly observed under the contact points. Greatest
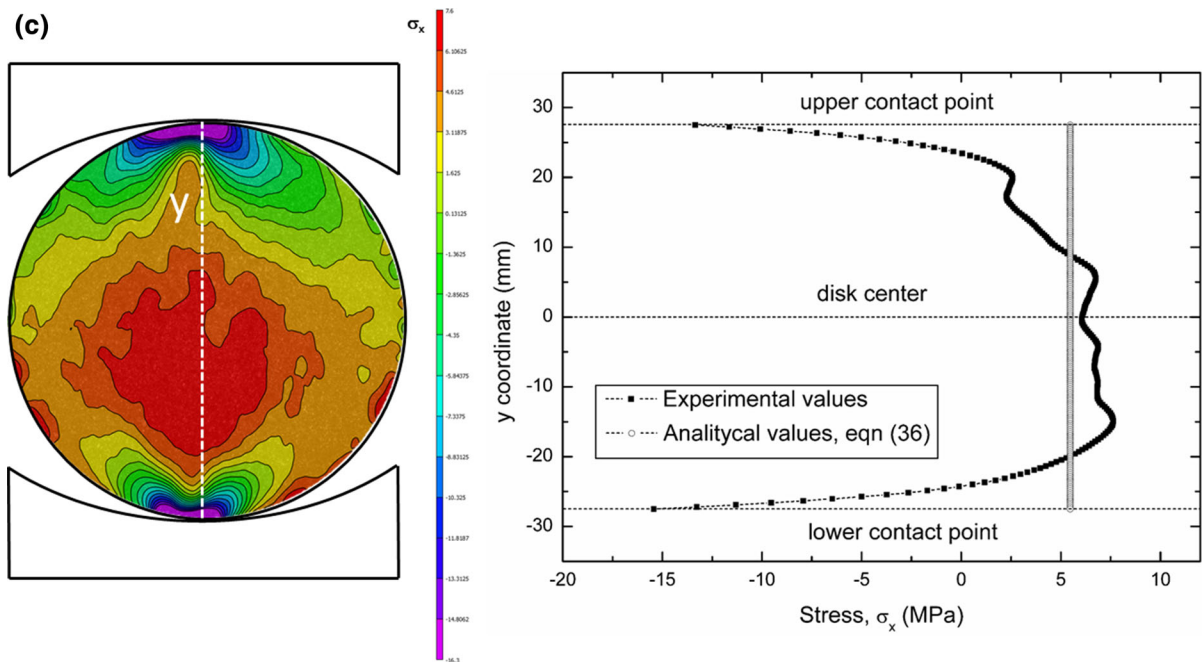
Fig. 5 continued

vertical compressive strain occurs exactly at the edges of the disc, whereas horizontal extension is located inward of these areas.

Figure S5b show that when rod platens are used, there are two regions, close to the contact point, where both the horizontal tensile stress and the vertical compressive stress are dominant. These values result higher than those recorded with the ASTM platens and, in particular, the horizontal tensile stress exhibits an extremely localized trend. This behavior, is the responsible of the premature failure of the samples.

Finally, for the ISRM loading method, Figure S5c, horizontal extension and associated vertical compression can be observed in the inner area of the disk. Areas of greatest compression are located to the top and bottom of the disc, as shown in the ASTM method. However, with the use of curved platens, these latter seem to show an eccentric behavior that, as also been observed by several authors [15], it is related to an imperfect interface between the sample curvature and that of the loading platen.

Overall, local stress analysis confirmed that curved platens represent the most suitable loading configuration for the evaluation of the tensile strength of brittle materials.

6 Conclusions

An optimized methodology for the complete mechanical characterization of brittle materials, based on the Brazilian disk test and the application of the Digital Image Correlation method, is proposed in this paper.

In particular, a special routine, which makes use of an over-deterministic method and the least square regression, was developed in order to estimate the mechanical elastic properties, i.e. the Young modulus and the Poisson ratio, and to fit the experimental displacement field. The routine is also able to automatically calculate error sources such as center of the disk location and rigid-body motion components, and delete their effect on the final solution.

The accuracy of the proposed approach was demonstrated by experiments performed on geopolymeric samples, and three different loading platens (flat, rod and curved platens) were used to investigate the effect of the loading conditions on the mechanical properties. It was demonstrated that loading conditions do not significantly affect the elastic constants calculation and results are in good agreement with those obtained with a conventional four points bending test.

In addition, starting from the measure strain and the computed elastic properties, local stress analysis, immediately before failure, was performed in order to evaluate the failure mechanisms involving the different loading configurations and the effective strength of the samples. Results revealed that the curve platens represent the most suitable loading condition for the tensile strength evaluation because they guarantee the lowest stress concentration at the loading points and a stress profile in good agreement with the analytical prediction.

The proposed methodology is easy to implement because it doesn't need stringent experimental requirements and allows to calculate Young's modulus, Poisson's ratio and the effective tensile strength of brittle materials in a single experiment where the driving force is represented by the determination of the full displacement fields experienced by a disk under compression.

Compliance with ethical standards

Conflict of interest The authors declare that they have no conflict of interest.

Ethical approval This chapter does not contain any studies with human participants or animals performed by any of the authors.

References

1. Carneiro FLLB (1943) A new method to determine the tensile strength of concrete. Paper presented at the proceedings of the 5th meeting of the Brazilian association for technical rules, 3d. section
2. Akazawa T (1943) New test method for evaluating internal stress due to compression of concrete: the splitting tension test. J Jpn Soc Civ Eng 29:777–787
3. ASTM C496 (1984) Standard test method for splitting tensile strength of cylindrical concrete specimens, vol 0.042. Annual Book of ASTM, Standards. ASTM, Philadelphia, pp 336–341
4. Fairhurst C (1964) On the validity of the 'Brazilian' test for brittle materials. Int J Rock Mech Min Sci Geomech Abstr 1(4):535–546
5. Hooper JA (1971) The failure of glass cylinders in diametral compression. J Mech Phys Solids 19(4):179–200
6. Hudson JA, Brown ET, Rummel F (1972) The controlled failure of rock discs and rings loaded in diametral compression. Int J Rock Mech Min Sci Geomech Abstr 9(2):241–248
7. Swab JJ, Yu J, Gamble R, Kilczewski S (2011) Analysis of the diametral compression method for determining the tensile strength of transparent magnesium aluminate spinel. Int J Fract 172:187–192
8. Li Diyuan, Wong Louis Ngai Yuen (2016) The Brazilian disc test for rock mechanics application: review and new insight. Rock Mech Rock Eng 46:269–287
9. Wang QZ, Jia XM, Kou SQ, Zhang ZX, Lindqvist PA (2004) The flattened Brazilian disc specimen used for testing elastic modulus, tensile strength and fracture toughness of brittle rocks: analytical and numerical results. Int J Rock Mech Min Sci 41:245–253
10. ISRM (1978) Suggested methods for determining tensile strength of rock materials. Int J Rock Mech Min Sci 15(3):99–103
11. Cardenas-Garcia JF (2001) The Moiré circular disc: two inverse problems. Mech Res Commun 28(4):381–387
12. Wang Z, Cardenas-Garcia JF, Han B (2004) Inverse method to determine elastic constants using a circular disk and Moiré interferometry. Exp Mech 45(1):27–34
13. Khlifi I, Dupré JC, Doumalin P, Belrhiti Y, Pop O, Huger M (2017) Improvement of digital image correlation for the analysis of the fracture behaviour of Refractories. In: 23ème Congrès Français de Mécanique, Lille, 28 Aug–Sept 2017
14. Lai S, Shi L, Fok A, Li H, Sun L, Zhang Z (2017) A new method to measure crack extension in nuclear graphite based on digital image correlation. Sci Technol Nucl Install 2017:1–10
15. Stirling RA, Simpson DJ, Davie CT (2013) The application of digital image correlation to Brazilian testing of sandstone. Int J Rock Mech Min Sci 60:1–11
16. Liu C (2010) Elastic constants determination and deformation observation using Brazilian disk geometry. Exp Mech 50:1025–1039
17. Hild F, Roux S (2006) Digital image correlation: from displacement measurement to identification of elastic properties—a review. Strain 42:69–80
18. Timoshenko S, Goodier J (1970) Theory of elasticity, 3rd edn. McGraw-Hill Book Company, Inc, New York
19. Markides ChF, Pazis DN, Kourkoulis SK (2010) Closed full-field solutions for stresses and displacements in the Brazilian disk under distributed radial load. Int J Rock Mech Min Sci 47:227–237
20. Kourkoulis SK, Markides ChF, Chatzistergos PE (2012) The Brazilian disc under parabolically varying load: theoretical and experimental study of the displacement field. Int J Solids Struct 49:959–972
21. Muskhelishvili HN (1958) Some basic problems in mathematic elastic mechanics (Translated by Zhao Huiyuan). Science Press, Beijing
22. Davidovits J (1982) Mineral polymers and methods for making them, US Patent 4; 349,386
23. Lamuta C, Candamano S, Crea F, Pagnotta L (2016) Direct piezoelectric effect in geopolymeric mortars. Mater Des 107:57–64
24. Duxson P, Fernández Jiménez A, Provis JL, Lukey GC, Palomo A, van Deventer JSJ (2007) Geopolymer

technology: the current state of the art. J Mater Sci 42:2917–2933

25. C. Solutions (2009) VIC-2D Testing Guide
26. ASTM C 1161-02c (2003) Standard test method for flexural strength of advanced ceramics at ambient temperature
27. Ajovalasit A (2006) Analisi Sperimentale delle tensioni con gli estensimetri elettrici a resistenza. Aracne Editrice S.r.l, Roma